Electrochimica Acta 68 (2012) 192–197

Contents lists available at SciVerse ScienceDirect

Electrochimica Acta

journal homepage: www.elsevier.com/locate/electacta

Oxygen reduction reaction on tantalum oxide-based catalysts prepared from TaC and TaN

Yoshiro Ohgi [a], Akimitsu Ishihara [a,*], Koichi Matsuzawa [a], Shigenori Mitsushima [a], Ken-ichiro Ota [a], Masashi Matsumoto [b], Hideto Imai [b]

[a] Chemical Energy Laboratory, Yokohama National University, Yokohama 240-8501, Japan
[b] NISSAN ARC Ltd., 1 Natsushima-cho, Yokosuka 237-0061, Japan

ARTICLE INFO

Article history:
Received 26 October 2011
Received in revised form 16 February 2012
Accepted 17 February 2012
Available online 25 February 2012

Keywords:
PEFC
ORR
Cathode
Oxide
Electrocatalyst

ABSTRACT

To obtain insights into the roles of carbon and nitrogen contained in the starting materials in partially oxidized tantalum carbonitride (TaC_xN_y) oxygen-reduction electrocatalysts, we studied oxygen-reduction-reaction (ORR) behaviors and structural properties of tantalum-oxide-based catalysts prepared by partial oxidation of tantalum carbides (TaC) and nitrides (TaN) under low oxygen pressure with 2%H_2/N_2 based gas at 1000 °C. The surface tantalum-oxide phase obtained from TaC were β-Ta_2O_5 in whole degree of oxidation (DOO) range, while the both TaON and Ta_2O_5 were formed in the surface phases obtained by the oxidation of TaN, especially at low DOO regions. The highest ORR response was obtained for β-Ta_2O_5 containing partially oxidized TaC (Ta—COs). Although, the local structure of surface oxide phase of β-Ta_2O_5 containing partially oxidized TaN (Ta—NOs) are almost identical, Ta—NOs showed no significant ORR responses. Carbon contained in the starting materials, therefore, plays an indispensable role in emergence of ORR activity.

1. Introduction

Polymer electrolyte fuel cells (PEFCs) are a key energy device in the next generation green technology having a wide variety of potential applications such as residential, portable and automotive power sources due to their high efficiency for energy conversion, low pollutant emission, and high-energy capacity. There are, however, technological issues to be overcome before the widespread commercialization of PEFCs, especially in the field of the cathode-catalyst development. Although platinum-based oxygen reduction reaction (ORR) catalysts are used as the best catalyst for cathodes of PEFCs at present, their innegligible over-potentials for ORR, the limited resources, or instability to strong acidic and high potential cathode conditions, limits practical uses of PEFCs. Thus, better ORR catalysts with higher activity, higher stability, and lower cost, preferably with non-platinum group materials, are strongly required.

While many studies have been done to develop non-platinum cathode catalysts for PEFCs, such as cobalt or iron-based macrocyclic complexes (N_4-chelate type such as phtalocyanines, porphyrins, and tetraazaanulens) [1–3], metal chalcogenides ($Mo_xRu_ySe_z$, Ru_xX_y (where X = S, Se, and Te)) [4–8], and carbon-based catalysts [9–11], these compounds are, actually, unstable in acidic and oxidizing atmosphere, and less-stable than that of platinum based cathode catalysts [11–17].

In contrast, we have been focusing on the materials' stability to sever cathode conditions, viz., strong acidic and corrosive environments, and have developed the groups 4 and 5 metal-oxide-based catalysts that have high ORR activities that are comparable to that of platinum, simultaneously exhibiting highly tolerant behaviors for the PEFC cathode condition [18–24]. The results of our studies on transition-metal-oxide-based ORR catalysts have suggested that the best ORR activity is obtained when transition-metal carbonitrides, such as TaC_xN_y, ZrC_xN_y, NbC_xN_y, are partially oxidized. Since the transition metal oxides themselves show no remarkable ORR activity, carbon and/or nitrogen that are included in the starting materials should play a role in emergence and enhancement of ORR activity of oxide-based ORR catalysts, although ORR active sites are actually in oxide phases instead of TaC or TaN phases.

In this research, to gain insights into such important roles of carbon and nitrogen involved in the starting materials, we studied ORR activities and structural properties of partially oxidized tantalum carbide (TaC) and tantalum nitrides (TaN), viz., end materials, with different degree of oxidation via electrochemical, X-ray diffraction and X-ray absorption measurements. The results suggested that carbon in the starting materials is indispensable for the emergence of ORR activity for catalysts with Ta_2O_5 phase, while N is necessary for ORR in TaON-based phase.

* Corresponding author.
E-mail address: a-ishi@ynu.ac.jp (A. Ishihara).

0013-4686/$ – see front matter © 2012 Elsevier Ltd. All rights reserved.
doi:10.1016/j.electacta.2012.02.059

2. Experimental

2.1. Synthesis of electrocatalysts

Tantalum carbide (TaC, ca. 1 μm) and tantalum nitride (TaN, ca. 2 μm) powders were obtained from Wako Pure Chemicals Co., Japan. These TaC and TaN powders were oxidized by heating at 1000 °C for 2–60 h under 2%H_2/N_2 containing 0.05–0.5%O_2 with gas flow rates of 20–100 cm^3 min^{-1} in a homemade rotary quartz tube furnace (SUNTECH CORPORATION, Japan). The degree of oxidation was controlled by changing the oxidation duration. We describe the partially oxidized tantalum carbides powders and nitrides powders as Ta—COs and Ta—NOs, respectively.

2.2. Electrochemical measurements

To maintain the electrical contact between the electrode and the nearly insulating Ta—CO and Ta—NO powders, fine Ketjen Black EC 300J powders (7 wt%) were added [18,22]. The catalyst ink was made by dispersing the catalyst and Ketjen Black powder (30 mg) in 1.5 mL of distilled water and isopropanol (mass ratio; 1–1). Then, obtained ink (ca. 2 mg) was dropped onto a glassy carbon (GC) rod (5.2 mm in diameter, Tokai Carbon Co., Japan) and it was covered with 10 μL of 0.5 wt% recast Nafion® solution. Electrochemical measurements were conducted with a three-electrode cell in oxygen or nitrogen saturated 0.1 mol dm^{-3} (M) H_2SO_4 at 30 °C using a PS08 potentiostat (TOHO Technical Research, Japan). A reversible hydrogen electrode (RHE) and a GC plate were used as a reference and a counter electrode, respectively. Before the catalytic activity and stability measurements, the electrode surface was cleaned by repeating cyclic voltammetry scans under oxygen at a scan rate of 1 V s^{-1} from 0.05 to 1.2 V with 100 cycles in 0.1 M H_2SO_4 at 30 °C until cyclic voltammogram reached a steady state. Then, the catalytic activity for the ORR was measured by a cyclic voltammetry from 1.2 to 0.2 V at a sweep rate of 5 mV s^{-1} under oxygen or nitrogen. The ORR current (i_{ORR}) was determined by subtracting the current under nitrogen from that under oxygen. We defined the onset potential for the ORR (E_{ORR}) as the electrode potential at i_{ORR} = −0.2 μA cm^{-2}. A current density was based on the geometric surface area of the working electrode.

To confirm the validity of the static ORR current measurements, we also compared the ORR current obtained from the Rotating disk electrode (RDE) and static conditions for the Ta—CO sample with DOO_{CO} = 0.15. The RDE measurements were performed with a rotor (NIKKO KEISOKU, Japan) and the PS08 potentiostat. The RDE was an assembled with a tantalum-based catalyst powder-coated GC disk (6 mm diameter) mounted in a PTFE holder. The same catalyst ink was dropped on a GC disk electrode with the Ta based catalysts mixed with 7wt% KB of ca. 1 mg on GC (6 mm diameter) and covered with 0.5 wt% recast Nafion® solution. In a comparison experiment, the loading was decreased to avoid dropping from RDE. The RDE measurements were carried out under O_2 or N_2 saturated in 0.1 M H_2SO_4 at 30 °C. RHE and a GC plate were also used as a reference and a counter electrode, respectively.

The catalyst-coated GC disks were electrochemically cleaned by sweeping the potential from 0.2 to 1.0 V at a sweep rate of 50 mV s^{-1} under N_2 up to 100 cycles. For ORR studies, RDE voltammgram was recorded from 1.2 to 0.2 V at 5 mV s^{-1} with the rotation speed of the electrode at 1600 rpm.

2.3. Structural characterization

Identification of oxide-phases and crystal structure analysis of the Ta—CO and Ta—NO catalysts were performed by using X-ray diffraction (XRD) (XRD-6000, Shimadzu, Japan). The X-ray diffraction profiles were corrected with a 0.02° step from 15° to 85° in 2θ with Cu Kα radiation. The local structures around Ta atoms were characterized by X-ray absorption spectroscopy (XAS) using synchrotron radiation X-rays. XAS measurements were carried out at the beamline BL14B2 at SPring-8. To obtain structural information of the near surface regions, we used conversion-electron-yield (CEY) XAS in addition to the conventional transmission XAS [25]. Since the CEY–XAS detects the flux of He^+ ions produced by the electrons emitted from the near surface regions due to an Auger process, we can selectively analyze that local structure of near surface phases restricting the probing depth within the escape depth of the Auger electrons [26]. The probing depth of CEY–XAS for a Ta L_3-edge was estimated to be 28.5 nm for β-Ta_2O_5 (density: 8.73 g cm^{-3}) [27].

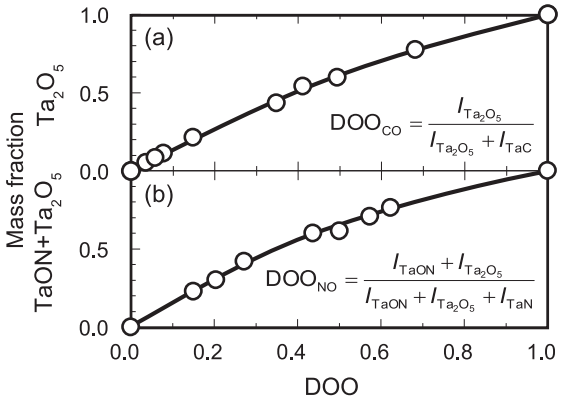

Fig. 1. Relationship between degree of oxidation (DOO) and mass fraction which is simulated from XRD patterns for Ta—CO system (a) and Ta—NO system (b). The definition of DOO for Ta—COs and Ta—NOs is given in the inset.

2.4. Definition of degree of oxidation

Degree of oxidation (DOO) was defined by using XRD intensities for the specific reflections, similar to the previous work [22]. As discussed in detail later, for Ta—CO system, the starting material TaC and the oxidized Ta_2O_5 phases coexisted. While, for Ta—NO system, TaON phase was formed in addition to TaN and β-Ta_2O_5 phases. Thus, we need to use different DOO definition for Ta—CO and Ta—NO.

The DOO for Ta—COs which consists of TaC and β-Ta_2O_5 phases is defined as,

$$DOO_{CO} = \frac{I_{Ta_2O_5}}{I_{Ta_2O_5} + I_{TaC}},$$

by using integrated intensity of 1 1 1 reflection of cubic (c) TaC and 0 1 1 1 reflection of orthorhombic (o) Ta_2O_5, and the DOO for Ta—NOs which contain TaN, Ta_2O_5, and TaON is defined as,

$$DOO_{NO} = \frac{I_{TaON} + I_{Ta_2O_5}}{I_{TaON} + I_{Ta_2O_5} + I_{TaN}},$$

by using integrated intensity of 1 1 0 reflection of hexagonal (h) TaN and 0 1 1 1 reflection of o-Ta_2O_5, and 1 1 $\bar{1}$ reflection of monoclinic TaON.

3. Results and discussion

3.1. X-ray diffraction

While we can easily evaluate oxide phase ratio in samples by the degree of oxidation (DOO) as defined above, there is a difference between the DOO and the mass fraction. Fig. 1 shows relation between degree of oxidation and mass fraction which was simulated from actual XRD patterns for Ta—CO system and Ta—NO

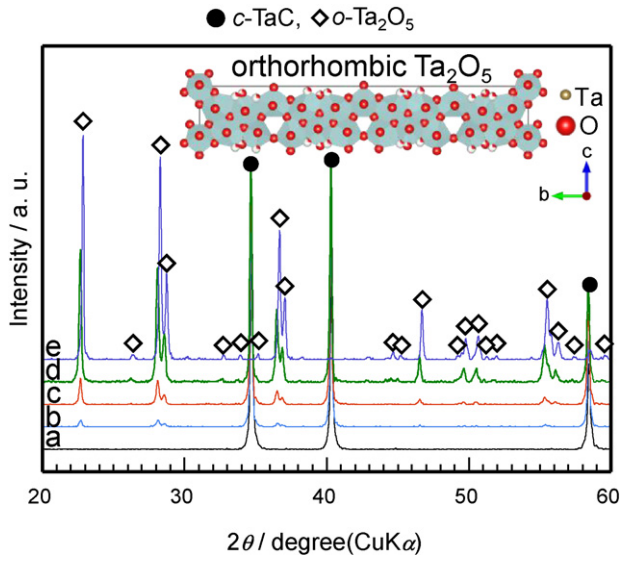

Fig. 2. Powder X-ray diffraction patterns of TaC and Ta—CO prepared at 1000 °C with DOO_{CO} of 0.0 (a), 0.06 (b), 0.15 (c), 0.41 (d) and 1.0 (f). Inset: the crystal structure of orthorhombic β-Ta_2O_5 [ICDD: 25-0922].

system. For Ta—CO system, mass fraction as shown in vertical axis contains only Ta_2O_5, while, for Ta—NO system, the fraction contains both TaON and Ta_2O_5. We can observe similar relation between DOO and mass fraction for Ta—CO and Ta—NO systems in Fig. 1(a) and (b). Then we can use DOO as a parameter helpful in estimating phase ratio of the formed phase during treatment.

Fig. 2 shows powder X-ray diffraction patterns of Ta—COs prepared at 1000 °C which correspond with DOO_{CO} values of 0.0 (a), 0.06 (b), 0.15 (c), 0.41 (d), and 1.0 (e). We observed only orthorhombic β-Ta_2O_5 phase (see the inset of Fig. 2) in the partial oxidation under present condition. This behavior is similar to the case for the partial oxidation process of TaC_xN_y systems [22].

Fig. 3 shows powder X-ray diffraction patterns of the Ta—NOs prepared at 1000 °C which correspond with DOO_{NO} values of 0.0 (a), 0.20 (b), 0.27 (c), 0.44 (d), and 0.57 (e). In contrast with Ta—COs and Ta—CNOs, tantalum oxynitride (TaON, see the inset of Fig. 3) were formed at rather lower intermediate DOO regions. To

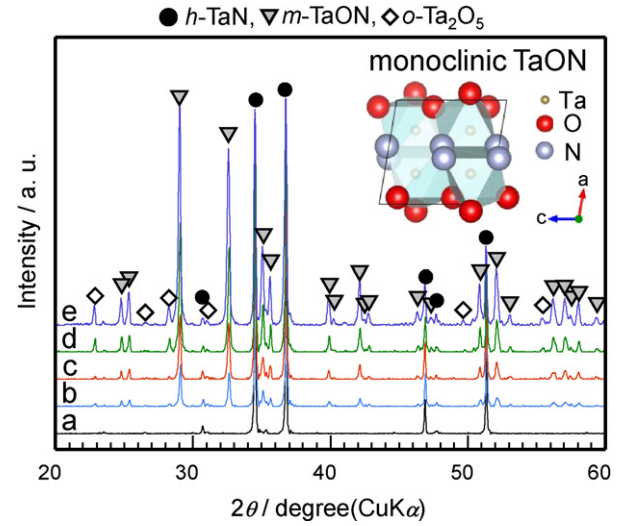

Fig. 3. Powder X-ray diffraction patterns of TaN and Ta—NO prepared at 1000 °C with DOO_{NO} of 0.0 (a), 0.20 (b), 0.27 (c), 0.44 (d), and 0.57 (e). Inset: crystal structure of monoclinic TaON [ICDD: 20-1235]. TaON was formed as a meta-stable phase in the oxidation process of TaN.

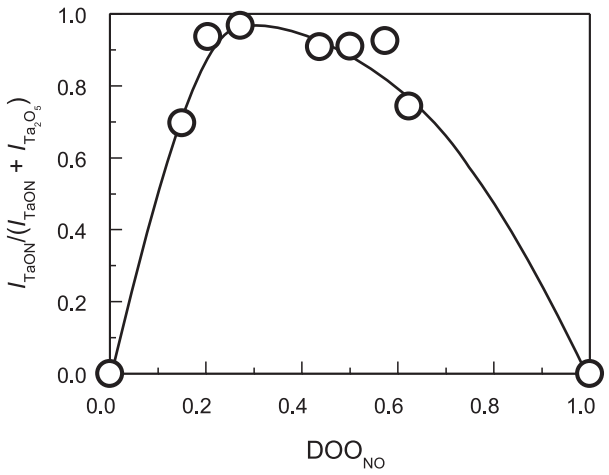

Fig. 4. DOO_{NO} variations of TaON ratio to Ta_2O_5 in Ta—NOs. The oxide phase contained almost only TaON at DOO_{NO} = 0.27.

roughly estimate the ratio of TaON to Ta_2O_5, we plot $I_{TaON}/(I_{TaON} + I_{Ta_2O_5})$ (I_{TaON}: integrated peak intensity for $1\,1\,\bar{1}$ reflection, $I_{Ta_2O_5}$: integrated peak intensity for $0\,1\,1\,1$ reflection), with respect to DOO_{NO}, in Fig. 4. The ratio of TaON reached a maximum around DOO_{NO} = 0.27, then, tantalum oxynitride gradually transformed to β-Ta_2O_5 as DOO increased. This suggests that thermodynamically the most stable phase in this synthesis condition is β-Ta_2O_5, but TaON can be formed as a meta-stable phase in the oxidation process under low oxygen partial pressure.

3.2. Catalytic activity for ORR

Fig. 5 shows potential–current curves (a) and Tafel plots (b) for Ta—CO with DOO_{CO} = 0.15 measured by using RDE with a rotating speed of 1600 rpm and a static electrode. We can see that the ORR activity obtained by the static measurement is in a good agreement with that obtained from a RDE measurement at higher potential as shown in Fig. 5(a) and (b). This result indicates that the dominant rate-determining step at higher potential regions is charge-transfer processes, and thus, there is little difference between the ORR activity determined from static and RDE measurements at higher potential. In this paper, we will discuss ORR activity with E_{ORR} and i_{ORR} at 0.8 V measured by only static measurements.

Fig. 6 shows voltammogram of TaC and Ta—CO systems (DOO_{CO} = 0.0, 0.15, 1.0) in 0.1 mol dm^{-3} at 30 °C with scan rate of 5 mV s^{-1}. Highly active Ta—CO was only shown in Fig. 6. TaC (a starting material) indicated a poor ORR activity. Similarly, the activity of complete oxides for both systems with DOO = 1 is less than those for the starting materials. In contrast to the starting materials and the complete oxides, the Ta—COs with intermediate DOO values had a higher activity.

The ORR activity of all samples was plotted against DOO. In Fig. 7(a) and (b), we plot the onset potential for the ORR, E_{ORR}, and the oxygen reduction reaction current, i_{ORR} at 0.8 V vs. RHE, for Ta—COs with respect to DOO_{CO}. (E_{ORR} and i_{ORR} for TaC and commercial Ta_2O_5 are also shown as references) The starting material, TaC, and commercial Ta_2O_5 showed no remarkable ORR activity: E_{ORR} of TaC and commercial Ta_2O_5 was about 0.5–0.6 V vs. RHE, and i_{ORR} at 0.8 V of TaC and commercial Ta_2O_5 was not positively observed, both of which can be ascribed for the ORR from Ketjen Black that were mixed as an electrical conducting additive.

Ta—COs, on the other hand, exhibit clear catalytic activity for ORR. As Ta_2O_5 formed on the surface (as DOO_{CO} increases), both E_{ORR} and i_{ORR} rapidly increased. The E_{ORR} values were above 0.9 V, which is almost the highest value among non-platinum group

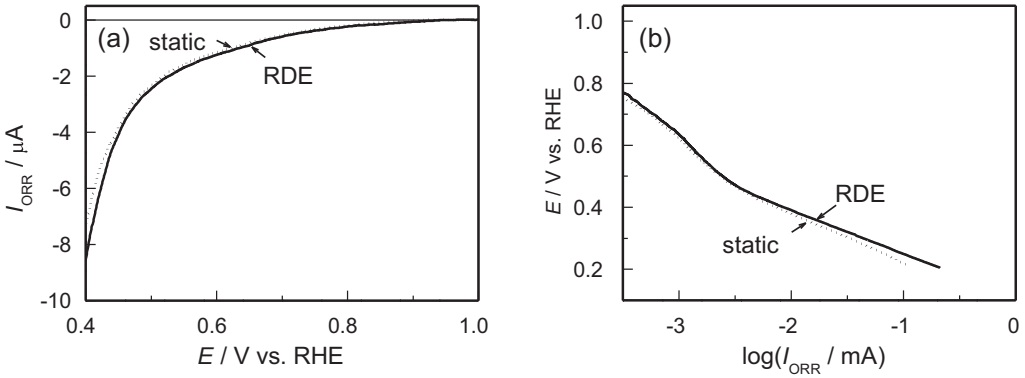

Fig. 5. Potential–current curves (a) and Tafel plots (b) for Ta—CO with DOO_{CO} = 0.15 measured in 0.1 mol dm^{-3} H_2SO_4 at 30 °C using RDE with a rotating speed of 1600 rpm (solid line), and static condition (dashed line). The loading of the catalyst + Ketjen Black mixture was ca. 1 mg on the test electrodes in this case. The current was raw data. Comparing results by RDE and static measurement, ORR activity is almost the same at higher potential for our catalyst.

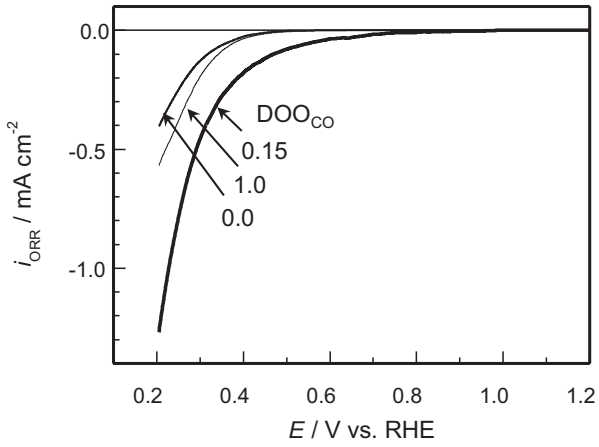

Fig. 6. Voltammogram of TaC and Ta—CO systems (DOO_{CO} = 0.0, 0.15, 1.0) in 0.1 mol dm^{-3} at 30 °C with scan rate of 5 mV s^{-1}.

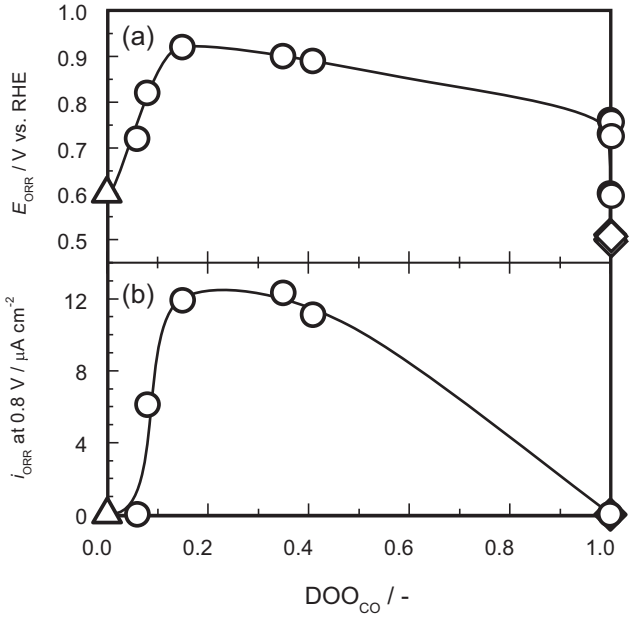

Fig. 7. ORR onset potentials for TaC (triangle), Ta—CO (circle) and commercial Ta_2O_5 (diamond). (b): ORR current i_{ORR} at 0.8 V vs. RHE. As DOO_{CO} increases up to 0.15, both E_{ORR} and i_{ORR} rapidly increased. Then the catalytic activity is almost saturated above DOO_{CO} = 0.15, and it again abruptly decrease at DOO_{CO} = 0.5.

ORR catalysts. Then the catalytic activity is almost saturated above DOO_{CO} = 0.15, and it again abruptly decrease at DOO_{CO} = 1.0.

The ORR behaviors of Ta—NOs are quite different from those of Ta—COs shown above. Fig. 8(a) and (b) show E_{ORR} and i_{ORR} for Ta—NOs. The starting material TaN have no ORR activity similar to TaC. In contrast with Ta—COs, the highest ORR activity is obtained only around DOO_{NO} = 0.27, and ORR activity, both E_{ORR} and i_{ORR}, rapidly decreased as DOO_{NO} increased. As revealed from XRD results (Fig. 3), the ratio of TaON reaches maximum at around DOO_{NO} = 0.27, indicating that TaON phase prepared by the present condition have intrinsic ORR activity, and Ta_2O_5 phase do not have ORR activity. Previously, we reported that TaON thin films prepared by reacting sputtering methods have ORR activity, and our present result showed TaON power prepared at low oxygen pressure could also work as ORR catalysts [23,28]. We consider that the high performance of Ta—NO with DOO_{NO} = 0.27 could be due to n-type semiconductive property of TaON which was mainly formed in Ta—NOs shown in Fig. 4 [29,30]. Another important finding is that β-Ta_2O_5 phase formed from TaN could not have ORR activity, while β-Ta_2O_5 phases formed from TaC or TaC_xN_y show rather extremely high ORR activity. Next, we will look at this difference by analyzing the local structure around Ta via XAS measurements.

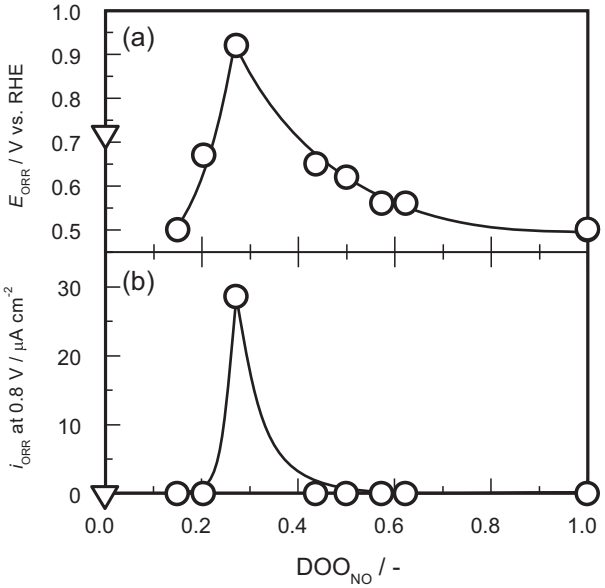

Fig. 8. Onset potentials for the ORR for TaN (reverse triangle) and Ta—NO (circle). (b): ORR current i_{ORR} at 0.8 V (b) against DOO_{NO}. The highest ORR activity is obtained at DOO_{NO} = 0.27.

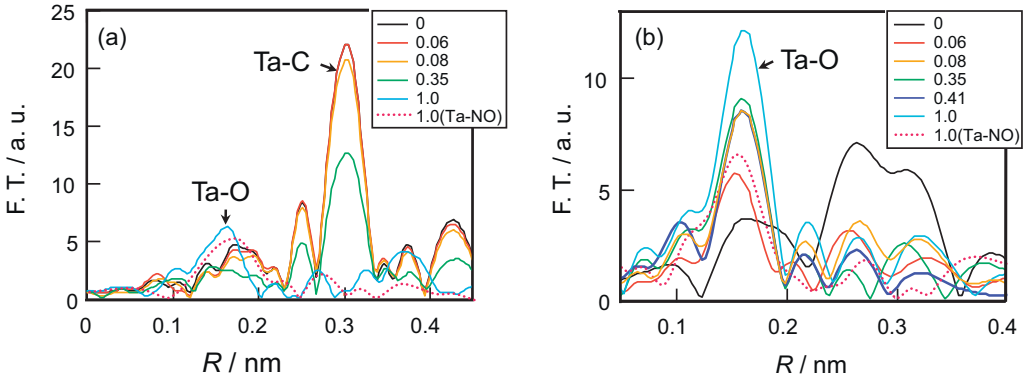

Fig. 9. Radial structure functions obtained from Fourier transform of EXAFS oscillation at Ta L_3 absorption edge for selected Ta—CO and Ta—NO catalysts, taken in transmission (a) and CEY (b) modes. In transmission mode, the radial structure functions have structural information on both surface oxides and inner TaC (or TaN). In contrast with transmission mode, we can see selectively surface regions of samples in the CEY mode. Peaks near 0.16 nm and 0.3 nm correspond to Ta—O bonds in Ta_2O_5, and Ta—C or TaN bonds in Ta-Carbonitrides, respectively. The surface region fully consists of tantalum oxides above $DOO_{CO} = 0.08$.

3.3. Local structure around Ta atoms analyzed by XAS

To analyze the local structure of near surface oxide-phases in partially oxidized Ta—COs and Ta—NOs, we conducted XAS measurements in both transmission and conversion-electron-yield modes [25]. Fig. 9(a) and (b) shows the radial structure functions obtained from Fourier transform of EXAFS oscillation at Ta L_3 absorption edge for selected Ta—CO and Ta—NO catalysts, taken in transmission and CEY mode, respectively.

Because transmission XAS probes an average structure of whole particles, the radial structure function obtained in a transmission mode have structural information on both surface oxides and inner TaC (or TaN). When looking at Fig. 9(a), thus, we can see that TaC were gradually oxidized and tantalum oxides were formed as a decrease in FT amplitude for Ta—C (or N) bonds, and as an increase in FT amplitude of Ta—O bonds in oxides.

CEY–XAS, on the other hand, selectively probes surface regions (ca. 28 nm below the surface). We see that, above $DOO_{CO} = 0.08$ (Ta—CO), the peak near 0.16 nm that is corresponding to Ta—O bonds in Ta_2O_5 is well grown: That is, the surface region fully consists of tantalum oxides above $DOO_{CO} = 0.08$. As demonstrated in a previous work, the amplitude of Fourier transform in the intermediate DOO_{CO} ranges ($0.08 < DOO_{CO} < 1$, the ORR active region) is smaller than that of DOO = 1 without ORR activity [25].

Fig. 10 illustrates the relationship between ORR activity and Fourier transform amplitude for at peak maximum in Ta—CO systems. The FT amplitude reflects the changing in density of oxygen vacancies in Ta_2O_5 structure. While ORR activity for Ta—CO with $DOO_{CO} = 1.0$ was low at high FT amplitude for Ta—O bond, both E_{ORR} and i_{ORR} have a behavior to increase with increase in the FT amplitude up to ca. 9. This indicates that tantalum oxides formed on TaC have oxygen vacancies, and such oxygen vacancies could work as active sites for ORR, suggesting that emergence of ORR activity originates in the same origin for Ta—CNO system.

The factors that enhance ORR activity is not only the existence of oxygen vacancies. As shown in Fig. 7(b), the FT amplitude for Ta—NO ($DOO_{NO} \sim 1$) that showed no remarkable ORR activity is smaller than that of Ta_2O_5 ($DOO_{CO} = 1$ for Ta—CO). This indicates that Ta—NO with Ta_2O_5-type surface oxides have oxygen vacancies that at potential ORR active sites, similar to ORR active Ta—CNO and Ta—CO, but oxygen vacancies in Ta—NO could not work well. Carbon contained in the starting materials should play an important role in enhancing ORR activity in addition to the creation of oxygen-vacancy defects. Let us see the effect of carbon with Raman spectroscopy.

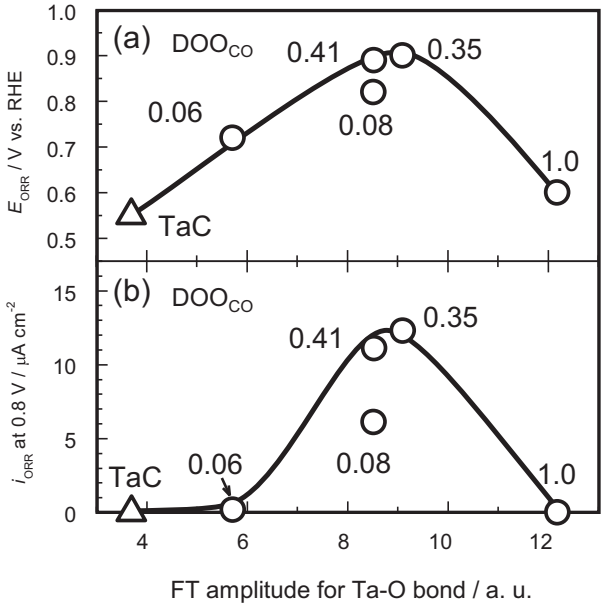

Fig. 10. Relationship between the ORR activity (the onset potential E_{ORR} (a), and ORR current i_{ORR} at 0.8 V (b)) and plotted Fourier transform amplitude. FT amplitude for Ta—O bond reflect the change in the density of oxygen vacancies in Ta_2O_5.

3.4. Raman spectroscopy

Fig. 11 shows Raman spectra of TaC and Ta—CO with $DOO_{CO} = 0.15$ (a) and TaN and Ta-NO with $DOO_{NO} = 0.27$ (b). For Ta—CO, two peaks that are ascribed for carbon with defect (G band (1585 cm^{-1}) for graphitic structure, and D band (1336 cm^{-1}) for defect structure) were clearly observed indicating carbon was generated during the partial oxidation process [31–33]. Carbon contained in the starting material TaC was precipitated on surface of the highly ORR active Ta—CO catalyst.

In contrast, no peak attributed to carbon was observed in Raman spectrum for Ta—NO. Thus, TaN and Ta—NO contained no carbon on the surface.

In the oxidation process of TaC, the carbon could be formed according to [34–36]

$$4TaC + 5O_2 \rightarrow 2Ta_2O_5 + 4C \quad (1)$$

Such carbon might mediate the electron transfer between electrode and active ORR sites that exist on the nearly insulating surfaces. Since such carbon should not exit in Ta—NO systems,

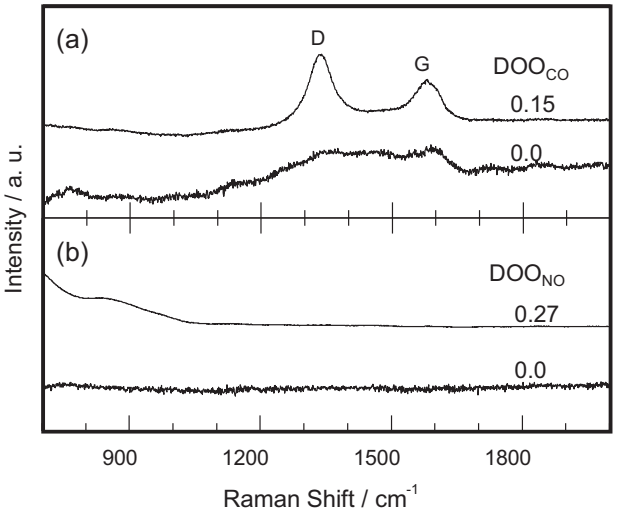

Fig. 11. Raman spectra of TaC and Ta—CO (DOO_{CO} = 0.15) (a) and TaN and Ta—NO (DOO_{NO} = 0.27) with measuring power of 6 mW at sample (b).

ORR does not effectively occur at nearly insulating surfaces. We are planning to investigate nature and roles of carbon species on the partially oxidized Ta—CNO and Ta—CO systems in near future.

We finally comment on the ORR activity observed in Ta—NO systems with near DOO_{NO} = 0.27. The crystal structure of this phase mainly contains TaON, oxynitride phase. As we previously reported, TaON thin films show ORR activity whose details are not clarified yet. Thus, TaON powders could also show ORR activity originating in similar mechanism that is different from ORR mechanism of Ta—CNOs and Ta—COs. We will plan to analyze local structures of such TaON catalysts soon.

4. Conclusion

In conclusion, we investigated ORR activity and structural properties of partially oxidized TaC and TaN via electrochemical measurements, X-ray diffraction, X-ray absorption spectroscopy, and Raman spectroscopy to understand the roles of carbon and nitrogen involved in the starting materials in Ta—CNO ORR catalysts prepared from TaC_xN_y.

Ta–oxide phases formed by partial oxidation of TaC had only orthorhombic Ta_2O_5 structure and oxygen-vacancy defects were introduced in the surface-oxide-phase. The ORR mechanism in this Ta—CO system is thus similar to that of Ta—CNOs. We also found that carbon involved in the carbonitride was deposited on the surface oxide phase. The surface phases formed on TaN, on the other hand, have both TaON and β-Ta_2O_5 phases. (TaON is a meta-stable phase, it transforms to β-Ta_2O_5 at high DOO_{NO} regions) Importantly, the β-Ta_2O_5 phases on the TaN show no remarkable ORR, although this phase also has oxygen-vacancies. In addition, carbon was not found at the surface of TaON and Ta_2O_5 formed from TaN. The details are not cleared yet, but we speculate that carbon involved in the starting materials (TaC or TaC_xN_y) is deposited during the partial oxidation process and provides electrical condition paths that are necessary for ORR to be effectively occurred.

We also found the TaON powders obtained as a meta-stable phase in the oxidation process had the ORR activity similar to TaON thin films, even though it did not contain carbon. Although the details are not clear at present, we expected hither ORR performance could be obtained based on the different ORR mechanism.

Acknowledgements

The synchrotron experiments, CEY–XAS measurements, were carried out on the BL14B2 beamline at SPring-8 under approval from the Japan Synchrotron Radiation Research Institute (JASRI) (Proposal Nos. 2009A1803, 2009B1821, 2009B2078, 2010B1009, 2010A1740, 2010A1748, 2010B1792, 2010B1888, 2011A1690, and 2011B5392). We thank the Grant-in-Aid for JSPS Fellow and New Energy and Industrial Technology Development Organization (NEDO) for financial support.

References

[1] R.J. Jasinski, Nature 201 (1964) 1212.
[2] O. Contamin, C. Debiemme-Chouvy, M. Savy, G. Scarbeck, J. New Mater. Electrochem. Syst. 3 (2000) 67.
[3] P. Convert, C. Coutanceau, P. Crouigneau, F. Gloaguen, C. Lamy, J. Appl. Electrochem. 31 (2001) 945.
[4] P. Gouerec, M. Savy, Electrochim. Acta 44 (1999) 2653.
[5] N. Alonso-Vante, H. Tributsch, Nature 323 (1986) 431.
[6] H. Tributsch, Catal. Today 39 (1997) 177.
[7] N. Alonso-Vante, I.V. Malakhov, S.G. Nikitenko, E.R. Savinova, D.I. Kochubey, Electrochim. Acta 47 (2002) 3807.
[8] D. Cao, A. Wieckowski, J. Inukai, N. Alonso-Vante, J. Electrochem. Soc. 153 (2006) A869.
[9] M. Chokai, M. Taniguchi, S. Moriya, K. Matsubayashi, T. Shinoda, Y. Nabae, S. Kuroki, T. Hayakawa, M. Kakimoto, J. Ozaki, S. Miyata, J. Power Sources 195 (2010) 5947.
[10] E.J. Biddinger, U.S. Ozkan, J. Phys. Chem. C 114 (2010) 15306.
[11] G. Liu, X. Li, P. Ganesan, B.N. Popov, Electrochim. Acta 55 (2010) 2853.
[12] G. Lalande, R. Cote, G. Tamizhmani, D. Guay, J.P. Dodelet, L. Dignard-Bailey, L.T. Weng, P. Bertrand, Electrochim. Acta 40 (1995) 2635.
[13] J. Maruyama, I. Abe, Chem. Mater. 17 (2005) 4660.
[14] E. Proietti, S. Ruggeri, J.P. Dodelet, J. Electrochem. Soc. 155 (2008) B340.
[15] A. Garsuch, K. MacIntyre, X. Michaud, D.A. Stevens, J.R. Dahn, J. Electrochem. Soc. 155 (2008) B953.
[16] X.G. Li, G. Liu, B.N. Popov, J. Power Sources 195 (2010) 6373.
[17] G. Liu, X. Li, J.W. Lee, B.N. Popov, Catal. Sci. Technol. 1 (2011) 207.
[18] Y. Ohgi, A. Ishihara, K. Matsuzawa, S. Mitsushima, K. Ota, J. Electrochem. Soc. 157 (2010) B885.
[19] A. Ishihara, Y. Ohgi, K. Matsuzawa, S. Mitsushima, K. Ota, Electrochim. Acta 55 (2010) 8005.
[20] Y. Ohgi, A. Ishihara, Y. Shibata, S. Mitsushima, K. Ota, Chem. Lett. 37 (2008) 608.
[21] Y. Maekawa, A. Ishihara, J.-H. Kim, S. Mitsushima, K. Ota, Electrochem. Solid-State Lett. 11 (2008) B109.
[22] A. Ishihara, Y. Shibata, S. Mitsushima, K. Ota, J. Electrochem. Soc. 155 (2008) B400.
[23] A. Ishihara, S. Doi, S. Mitsushima, K. Ota, Electrochim. Acta 53 (2008) 5442.
[24] Y. Shibata, A. Ishihara, S. Mitsushima, N. Kamiya, K. Ota, Electrochem. Solid-State Lett. 10 (2007) B43.
[25] H. Imai, M. Matsumoto, T. Miyazaki, S. Fujieda, A. Ishihara, M. Tamura, K. Ota, Appl. Phys. Lett. 96 (2010), 191905/1.
[26] A. Erbil, G.S. Cargill III, R. Frahm, R.F. Boehme, Phys. Rev. B 37 (1988) 2450.
[27] S.L.M. Schroeder, Solid State Commun. 98 (1996) 405.
[28] A. Ishihara, K. Lee, S. Doi, S. Mitsushima, N. Kamiya, M. Hara, K. Domen, K. Fukuda, K. Ota, Electrochem. Solid-State Lett. 8 (2005) A201.
[29] A. Kikuchi, A. Ishihara, Y. Ohgi, K. Matsuzawa, S. Mitsushima, K. Ota, M. Matsumoto, H. Imai, J. Japan Inst. Metals 75 (2011) 545.
[30] A. Ishihara, A. Kikuchi, Y. Ohgi, K. Matsuzawa, S. Mitsushima, K. Ota, M. Matsumoto, H. Imai, J. Japan Inst. Metals 75 (2011) 552.
[31] R.O. Dillon, J.A. Woollam, V. Katkanant, Phys. Rev. B Condens. Matter. 29 (1984) 3482.
[32] D. Beeman, J. Silverman, R. Lynds, M.R. Anderson, Phys. Rev. B Condens. Matter. 30 (1984) 870.
[33] L.C. Nistor, J. Van Landuyt, V.G. Ralchenko, T.V. Kononenko, E.D. Obraztsova, V.E. Strelnitsky, Appl. Phys. A A58 (1994) 137.
[34] M.W. Chase, J. Phys. Chem. Ref. Data 27 (1998).
[35] B.J. McBride, S. Gordon, M.A. Reno, Thermodynamic Data for Fifty Reference Elements, Lewis Res. Cent., Natl. Aeronaut. Space Adm., Cleveland, OH, USA, 1993, p. 240.
[36] I. Barin, O. Knacke, O. Kubaschewski, Thermochemical Properties of Inorganic Substances, 2nd ed., Springer-Verlag, Berlin, 1977.